Volume 16
Number 39
21 October 2025
Pages 17973–18462

Chemical Science

rsc.li/chemical-science

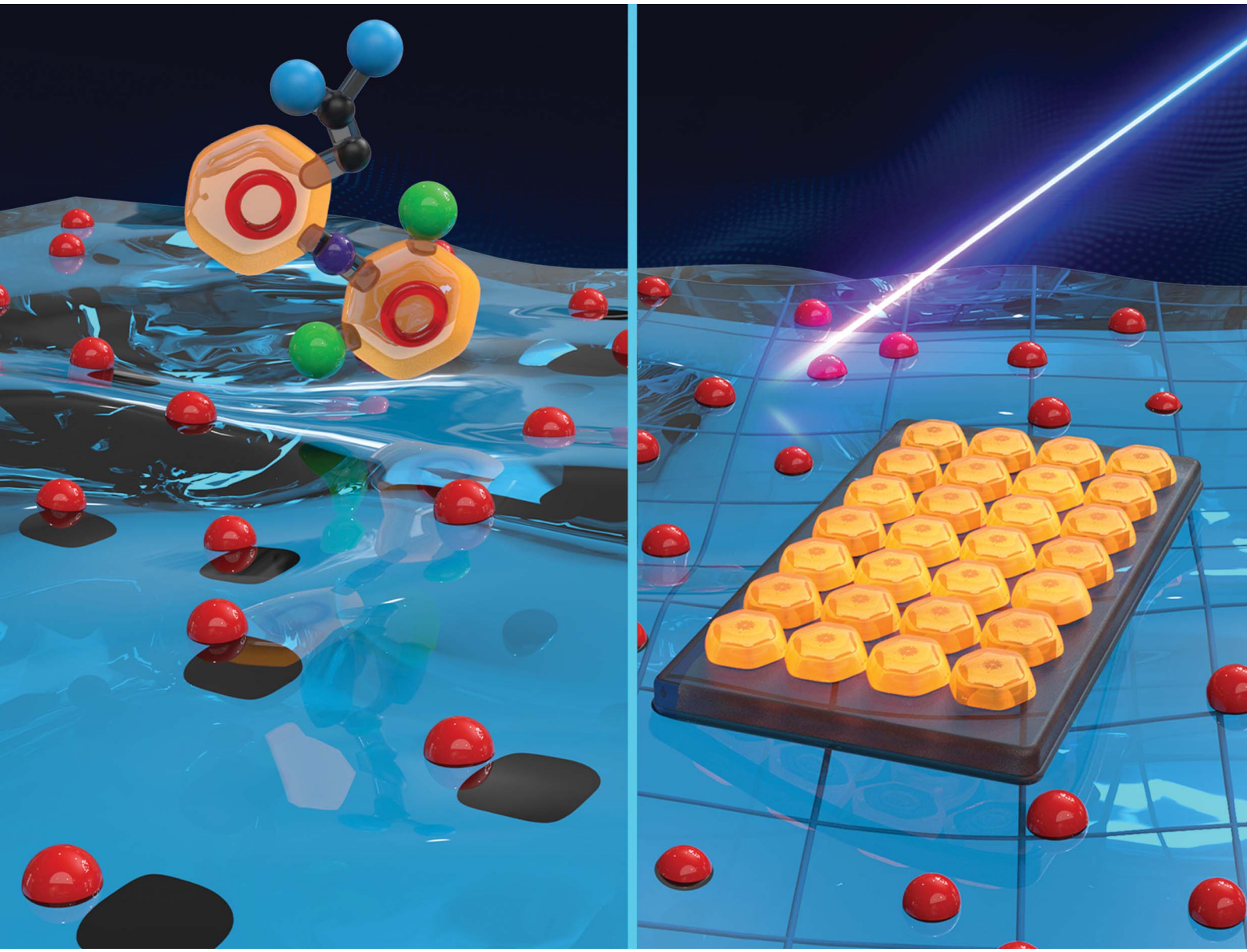

ISSN 2041-6539

ROYAL SOCIETY OF CHEMISTRY

EDGE ARTICLE
Hao Lu, Dirk Zahn, Mischa Bonn *et al.*
Promoting organic nucleation of diclofenac: hydrophobic interfacial interactions drive self-assembly

15 YEARS ANNIVERSARY

Chemical Science

ROYAL SOCIETY OF CHEMISTRY

EDGE ARTICLE

View Article Online
View Journal | View Issue

Check for updates

Cite this: *Chem. Sci.*, 2025, **16**, 18092

All publication charges for this article have been paid for by the Royal Society of Chemistry

Promoting organic nucleation of diclofenac: hydrophobic interfacial interactions drive self-assembly

Hao Lu, *[ab] Eduard Wiedenbeck,[c] Moritz Macht,[d] Daizong Qi,[b] Ali Dhinojwala,[e] Han Zuilhof,[fg] Dirk Zahn, *[d] Helmut Cölfen †[c] and Mischa Bonn *[b]

We compare the pH-triggered nucleation of the pharmaceutical diclofenac in bulk solution and at the air–water interface, using a combination of cryo-transmission electron microscopy, surface-specific spectroscopy and microscopy, and molecular dynamics simulations. In solution, simulation data reveal diclofenac forms dynamically ordered, liquid-like pre-nucleation clusters (PNCs), following a nonclassical nucleation pathway. At the air–water interface, nucleation occurs earlier during the titration process. The promoted nucleation is attributed to the interfacial enrichment of protons at this hydrophobic interface, elevated interfacial apparent pK_a for diclofenac, as well as the interface-induced ordered diclofenac–water structures. While hydrophobic interactions drive the first air–diclofenac–water layer, further diclofenac molecules tend to separate from water by forming hydrogen-bonded dimers, characteristic of the crystal structure. These findings provide molecular-level insights into organic nucleation, highlighting the importance of hydrophobic interfaces in controlling the process, with potential implications for various applications in pharmaceutical and materials science.

Received 26th May 2025
Accepted 1st September 2025

DOI: 10.1039/d5sc03816b

rsc.li/chemical-science

Open Access Article. Published on 03 September 2025. Downloaded on 17/5/2026 9:18:33 AM. This article is licensed under a Creative Commons Attribution-NonCommercial 3.0 Unported Licence.

1 Introduction

Organic nucleation is a highly relevant process in the pharmaceutical industry. The nucleation of active pharmaceutical ingredients (API) is central in medicinal chemistry since new crystal forms of API can lead to new therapeutic effects,[1,2] which are linked with enormous potential economic benefits, given the multi-billion dollar pharmaceutical industry. Understanding the nucleation mechanisms of APIs is a prerequisite for controlling the nucleation process, thereby achieving desirable crystal forms of API medicine.[3] Detailed insights into the nucleation of API crystals are therefore crucial. For the nucleation of organic molecules, early nucleation events determine the eventual fate of the precipitates, controlling the structural polymorphism, crystallite size, and shape.[4] Despite continuous efforts to understand the mechanism of organic nucleation, it still represents a challenge in chemistry.[5–8]

The nucleation process is often described by classical nucleation theory, which states that the nucleation will be thermodynamically favorable once the nucleus reaches a threshold size, and crystal growth occurs.[9–11] However, classical nucleation theory – mainly adapted for homogeneous nucleation – is often inaccurate in predicting the rates of the nucleation process. By contrast, nonclassical nucleation mechanisms have been proposed – stressing interfacial effects in heterogeneous nucleation. Two distinct nonclassical pathways have been demonstrated: two-step nucleation[3,12,13] and nucleation through pre-nucleation clusters (PNCs).[3,14] The former two-step pathway emphasizes a dense liquid phase, initially formed by liquid–liquid phase separation. In the second step, the crystal develops within the dense liquid phase.[12,13] The latter PNC pathway states that pre-nucleation is associated with the formation and evolution of thermodynamically PNCs. PNCs have been successfully invoked to describe different inorganic mineralizations, like calcium carbonate,[14] calcium oxalate,[15] iron (oxy)(hydr)oxides,[16] aluminum (oxy)(hydr)oxides,[17] and sodium chloride.[18] These PNCs rapidly form in the solution prior to nucleation, and their aggregation, as critically mediated by water,[19–23] triggers liquid phase separation, which results in further densification and solidification.

[a]College of Materials and Textile Engineering, G60 STI Valley Industry & Innovation Institute, Jiaxing University, Jiaxing, Zhejiang Province, 314001, China. E-mail: lu@zjxu.edu.cn

[b]Max Planck Institute for Polymer Research, Ackermannweg 10, 55128 Mainz, Germany. E-mail: bonn@mpip-mainz.mpg.de

[c]Department of Chemistry, University of Konstanz, Universitätsstrasse 10, Konstanz 78457, Germany

[d]Lehrstuhl für Theoretische Chemie/Computer Chemie Centrum, Friedrich-Alexander Universität Erlangen-Nürnberg, Nägelsbachstraße 25, 91052 Erlangen, Germany. E-mail: dirk.zahn@fau.de

[e]School of Polymer Science and Engineering, The University of Akron, Akron, OH 44325, USA

[f]College of Biological and Chemical Engineering, Jiaxing University, Jiaxing 314001, China

[g]Laboratory of Organic Chemistry, Wageningen University, 6708 WE Wageningen, The Netherlands

† This work is dedicated to Helmut Cölfen, who sadly passed away in 2024.

© 2025 The Author(s). Published by the Royal Society of Chemistry

Open Access Article. Published on 03 September 2025. Downloaded on 17/5/2026 9:18:33 AM.
This article is licensed under a Creative Commons Attribution-NonCommercial 3.0 Unported Licence.

Our recent study unveiled that nucleation of the organic pharmaceutical ibuprofen follows the PNC pathway, which, like inorganic nucleation, is mediated by water molecules.[24] Unlike inorganic minerals, organic molecules are often amphiphilic, providing both solubility in water/blood and migration of intestinal membranes, and there are static hydrophobic–hydrophilic patches on large organic molecular assemblies. In addition, the dynamic transient exposure of hydrophobic–hydrophilic regions often occurs. For nucleation of organic molecules (*e.g.* API), hydrophobic interfaces in an aqueous environment are the places where molecule assembly typically occurs. Those interfaces mimic the interfaces between PNCs and water, and thus are closely related to the formation and evolution of PNCs. Apparently, hydrophobic interfacial interactions are often considered the main driving force for organic nucleation.[25] Nevertheless, the specific role of hydrophobic interface – as stressed in nonclassical nucleation mechanisms – for tailoring organic nucleation has remained elusive, due to the challenge of characterizing this molecularly thin region.

In this work, we compare the nucleation of a representative API, diclofenac, in bulk solution and at the air–water interface, which is an excellent model hydrophobic interface.[24] The nucleation of diclofenac molecules in solution follows a nonclassical PNC pathway, as notably featured by the dynamically ordered liquid-like PNCs. In stark contrast, diclofenac and water form highly ordered localized structures at the air–water interface, the surface-enrichment of protons at this hydrophobic interface are likely to promote interfacial nucleation during titration process through neutralization by protonation of diclofenac. Our combined surface-specific sum frequency generation (SFG) and molecular dynamics (MD) simulation studies reveal that the assembly of interfacial diclofenac promotes nucleation by enhancing hydrophobic contacts and forming pair-wise hydrogen bonds, as characteristic of the dimer crystal structure.

2 Results and discussion

2.1 Nucleation of diclofenac in solution

Diclofenac is a weak organic acid, with pK_a of 4.16.[26,27] As illustrated in Fig. 1(A), protonation of the charged diclofenac sodium generates neutral diclofenac. Once neutral, the electrostatic repulsion stabilizing individual molecules in solution is lifted, and nucleation of diclofenac is triggered after supersaturation of diclofenac in solution.[28] To follow the protonation and subsequent nucleation, we performed a titration experiment using a recently developed double-dosing approach.[28,29] For this titration experiment, a 20 mM HCl solution was slowly and gradually dosed into a 5 mM diclofenac sodium solution, and a diclofenac sodium solution was simultaneously dosed to ensure nearly constant ionic strength (Fig. S1). A pH electrode monitored the solution pH. Fig. 1(B) shows the titration curve for the solution pH as a function of the added HCl volumes (V_{HCl}). The pH value decreases with increasing V_{HCl}, yet it increases slightly after V_{HCl} = 250 μL. With nucleation occurring, the introducing protons provided by adding HCl are not sufficient to compensate for the protons as consumed for nucleated diclofenac, which leads to decreased concentration and accordingly increased pH. In this context, the nucleation

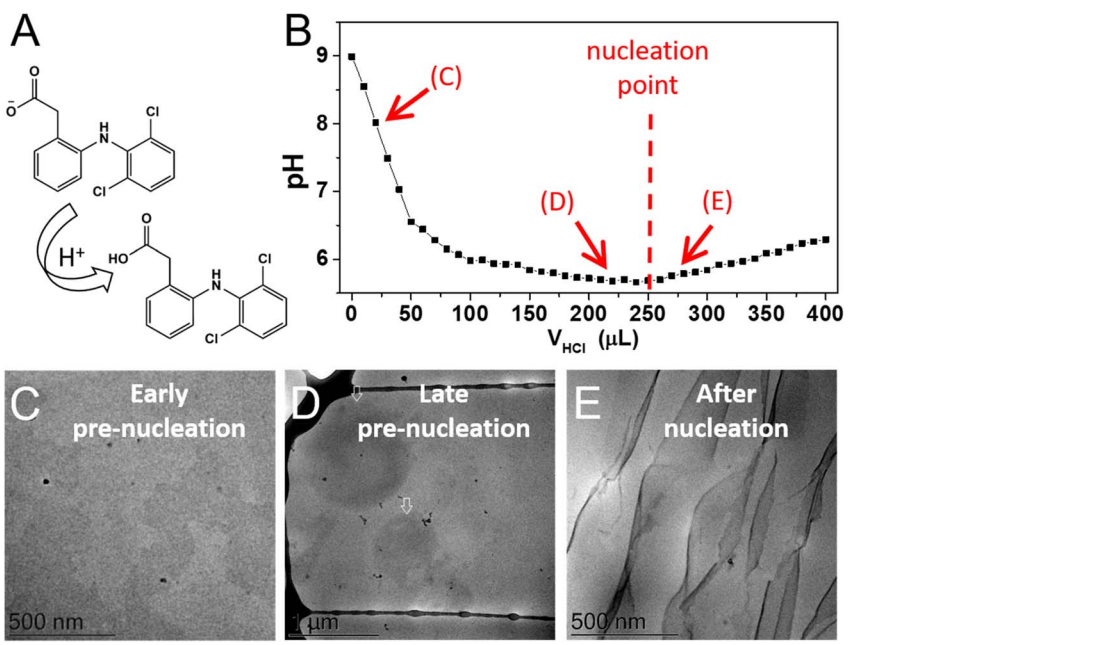

Fig. 1 Nucleation of diclofenac in solution. (A) Chemical structures of deprotonated diclofenac sodium and protonated diclofenac. (B) Titration curve: variation of the pH for diclofenac sodium solution with increasing HCl volume (V_{HCl}). The red dashed line marks the onset of nucleation (see text for details). (C–E) Cryo-TEM images of a vitrified sample of diclofenac at different nucleation stages as indicated in the titration curve: *i.e.* at early pre-nucleation (C), late pre-nucleation (D), and right after nucleation (E), respectively. The black areas and lines are the holes from the carbon grids, and the black objects are ice particles formed during the cryo-TEM measurement.

Open Access Article. Published on 03 September 2025. Downloaded on 17/5/2026 9:18:33 AM. This article is licensed under a Creative Commons Attribution-NonCommercial 3.0 Unported Licence.

occurs with dosing $V_{HCl} = 250$ μL, at which the solution pH starts to increase.[24]

We collect the diclofenac samples at different nucleation stages, as indicated as the positions of C, D, and E in the titration curve (Fig. 1(B)). We examine their structures *via* cryo-Transmission Electron Microscope (cryo-TEM), as shown, respectively, in Fig. 1(C–E). At the early pre-nucleation stage, inter-connected and roundish objects of ~200 nm diameter could be observed (Fig. 1(C)), while exhibiting rather low contrast. At late pre-nucleation prior to nucleation, separated circular structures were visible with improved contrast, yet with a larger size of 0.3–1.0 μm (Fig. 1(D)). After nucleation starts (*i.e.* $V_{HCl} > 250$ μL), abundant ribbon-like structures, as characteristic of nucleated solids,[22] can be clearly identified (Fig. 1(E)). The nucleated ribbon species (Fig. 1(E)) contrasts with the species at late pre-nucleation (Fig. 1(D)), which consolidates the nucleation point (*i.e.* $V_{HCl} = 250$ μL) as determined from the titration curve. The electron diffraction pattern from selected ribbon-rich area shows diffuse rings (Fig. S2), implying that the nucleated diclofenac lack a defined crystalline structure.

To investigate the diclofenac–water aggregates from MD simulations, we probed various concentrations to match the experimentally assessed density of 1.205 ± 0.004 g cm^{-3}. This density value was calculated based on data of analytical ultracentrifugation (Table S1), the measurement and calculation details for this method have been described in previous literature.[24,30] Fig. 2 illustrates the resulting system originally prepared as fully dispersed diclofenac molecules in water (1 : 10), followed by 50 ns MD simulation. The aggregation of diclofenac molecules and PNC formation is observed within about 20 ns. After this relaxation, we find a stable PNC solution – which reflects a dynamic equilibrium of aggregated diclofenac molecules in differently sized and shaped PNCs. For illustration of the dynamic character of the PNC solution, we discriminate

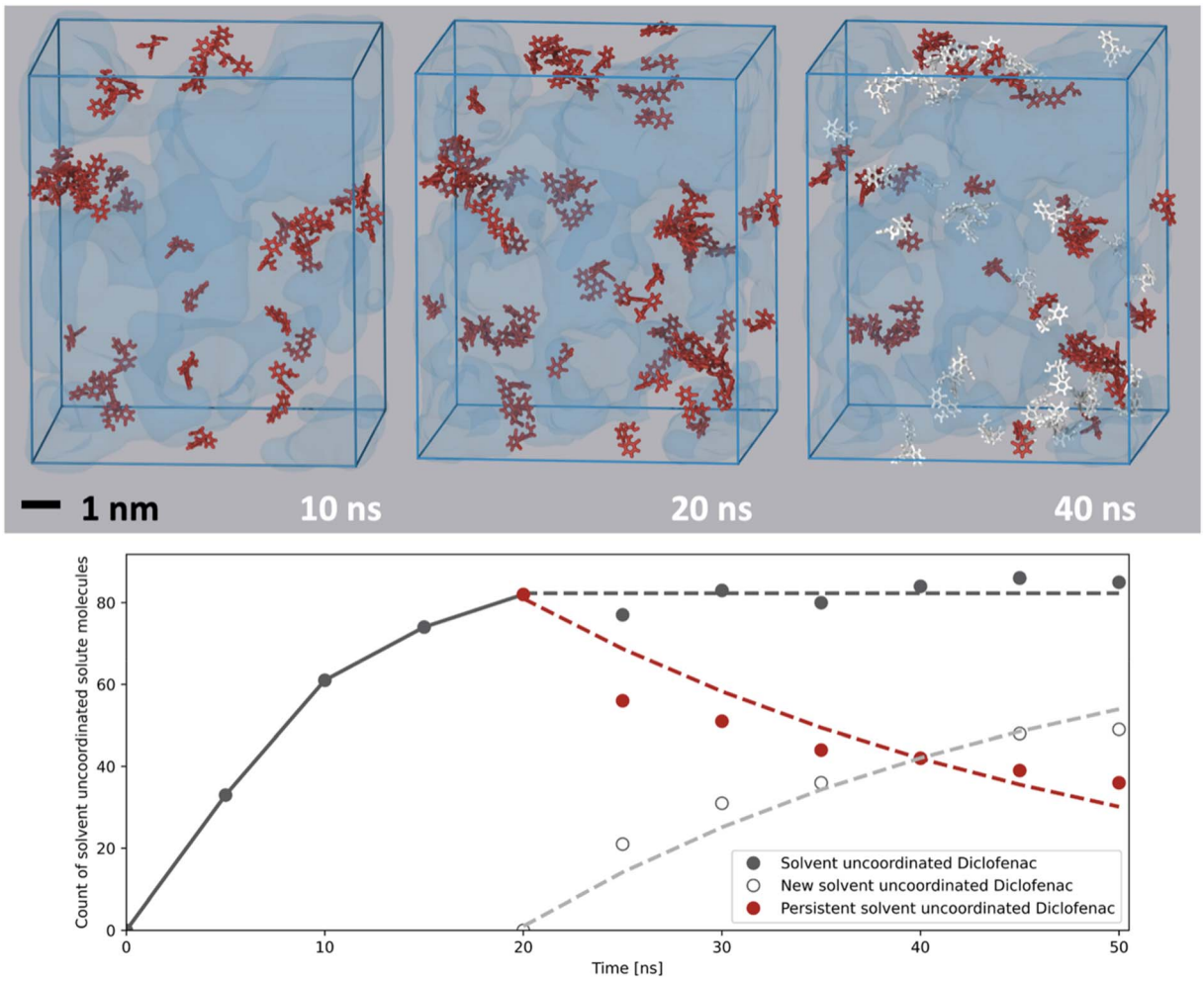

Fig. 2 Dynamically ordered diclofenac–water PNCs in solution. (top) Simulated structures of a (1 : 10) diclofenac solution in water. The structures, from left to right, illustrate the aggregation of diclofenac (10 ns), the fully aggregated liquid-like PNCs (20 ns), and the dynamic transition of PNCs (40 ns), respectively. Water is shown as transparent blue, whereas the forming aggregates (10 ns) and PNCs (20 ns) of diclofenac are colored in red and red/white to highlight the dynamics of the PNC (40 ns), respectively. (bottom) Number of water-uncoordinated diclofenac molecules (as compared to a total of 1210 solutes in the simulation cell) with increasing simulation time. Dark grey dots refer to the total number of de-solvated diclofenac molecules – which stays roughly constant upon 20 ns of relaxation from the random mixture. After 20 ns (dashed curves), our statistics of the water uncoordinated PNCs (dark gray) are divided into persistently uncoordinated diclofenac molecules (red) and newly uncoordinated solutes (light grey). Analogous coloring is used for the snapshots at 20 and 40 ns in the upper panel, respectively.

© 2025 The Author(s). Published by the Royal Society of Chemistry

Open Access Article. Published on 03 September 2025. Downloaded on 17/5/2026 9:18:33 AM.
This article is licensed under a Creative Commons Attribution-NonCommercial 3.0 Unported Licence.

diclofenac molecules that persistently remain water-uncoordinated within the PNCs formed at 20 ns (red), and those that were in contact with water at 20 ns, but become water-uncoordinated at later stages of the MD run (white). Notably, the observed dynamic transition for the PNCs of diclofenac is, to the best of our knowledge, the first report of the dynamic nature of pre-nucleation species in organic nucleation, which resembles those dynamically ordered liquid-like oxyanion polymer (dollop) in inorganic $CaCO_3$ mineralization.[31]

To quantify the dynamics of the evolving diclofenac–water PNCs, we calculate (i) the total number of water-uncoordinated diclofenac molecules as a function of simulation time, as presented in Fig. 2 (bottom). Upon 20 ns relaxation, this number reaches a plateau of ~80, which indicates convergence of the aggregation of diclofenac molecules. In the following 30 ns, the total of water-uncoordinated diclofenac molecules in PNCs remains unchanged (gray dots). However, the overall PNC solution reflects a dynamic equilibrium with the role of the involved diclofenac molecules changing on the 10 ns scale. Fits of first-order kinetics are shown for the number of molecules persistently residing within the PNC core (red curves) and those diclofenac species newly entering the PNCs core (grey curves/white in the snapshots of the upper panel). The exponential fits indicate a half-life time of ~30 ns for the exchange of diclofenac species in the PNC core and at its boundaries, respectively, which points out the highly dynamic nature of the PNCs.

2.2 Nucleation of diclofenac at the air–water interface

We combine surface pressure and Brewster Angle Microscopy (BAM) to monitor the nucleation of diclofenac at the air–water interface. Fig. 3(A) presents the variation of the surface pressure for the water surface of diclofenac sodium solution, titrating in HCl as in Fig. 1(B). Diclofenac sodium shows no surface activity without added HCl (0 μL). Immediately upon adding HCl (25 μL), the surface pressure value rises, and the value increases step-wise with each addition of HCl, which is mainly attributed to the higher surface activity of amphiphilic diclofenac molecules. We applied complementary BAM to monitor the morphology of the solution surface upon adding HCl. Fig. 3(B–D) presents the surface morphology after adding HCl volumes of 0 μL (B), 100 μL (C), and 250 μL (D), respectively. As clearly seen in Fig. 3(C), distinct nucleated flake species were observed with the addition of HCl of 100 μL. These sharp-edged features are drastically different from the circular-like shape for liquids,[25] and are comparable to the nucleated ribbon species in bulk solution. The identified flakes in BAM measurement exhibit much stronger contrast than liquids, suggesting their solid-like feature, which is typically associated with a higher change of refractive index for nucleated species at the interface. Notably, the HCl volume (100 μL) required for nucleation at the air–water interface is much lower than that (250 μL) for bulk solution – implying the promoted nucleation at the air–water interface.

2.3 Molecular structure and interaction for nucleation of diclofenac at the air–water interface

To gain mechanistic insights for promoted nucleation of diclofenac at the air–water interface, we apply surface-specific SFG spectroscopy to probe the structure and interaction between diclofenac and water during interfacial nucleation. In SFG

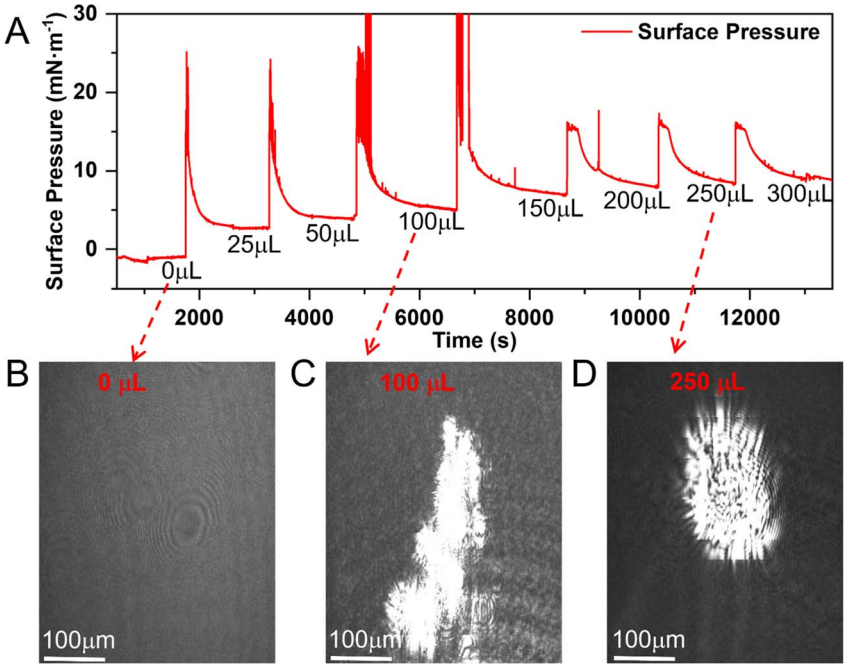

Fig. 3 Nucleation of diclofenac at the air–water interface. (A) Surface pressure variation for the water surface of a diclofenac sodium solution, with gradual dosing of HCl in accordance with the titration curve in Fig. 1(B). (B–D) BAM images for the solution surface with adding HCl volumes of 0 μL (B), 100 μL (C), and 250 μL (D), respectively.

Open Access Article. Published on 03 September 2025. Downloaded on 17/5/2026 9:18:33 AM. This article is licensed under a Creative Commons Attribution-NonCommercial 3.0 Unported Licence.

measurements, visible and infrared laser beams are overlapped at the interface both in time and space, generating photons at the sum frequency of the two beams. The SFG signal is enhanced when the IR beam is resonant with vibrational modes of interfacial molecules. The selection rules dictate that SFG signal is only generated from ordered molecules at the boundary interfaces where centrosymmetry is broken,[32–34] thereby excluding the signal contributions from the bulk solution.

We perform the SFG experiment once the surface pressure is in equilibrium. Fig. 4(A) shows the SFG spectra in the frequency range of 1540–1820 cm^{-1} for the diclofenac sodium at the air–water interface with varying pH, which are derived from the titration curve in Fig. 1(B). The spectrum for diclofenac sodium at pH = 9.0 does not show an observable SFG signal, which is in agreement with the zero surface pressure in Fig. 3(A). With decreasing pH, two distinct bands appear: one at ~1589 cm^{-1}, assigned to the antisymmetric COO^- stretch mode of the deprotonated COO^- group in diclofenac sodium; and the other at ~1720 cm^{-1}, assigned to the C=O stretch of the protonated COOH group in diclofenac. The presence of distinct COO^- and COOH peaks implies the substantial ordering of accumulated charged diclofenac sodium and neutral diclofenac at the air–water interface during the nucleation process.

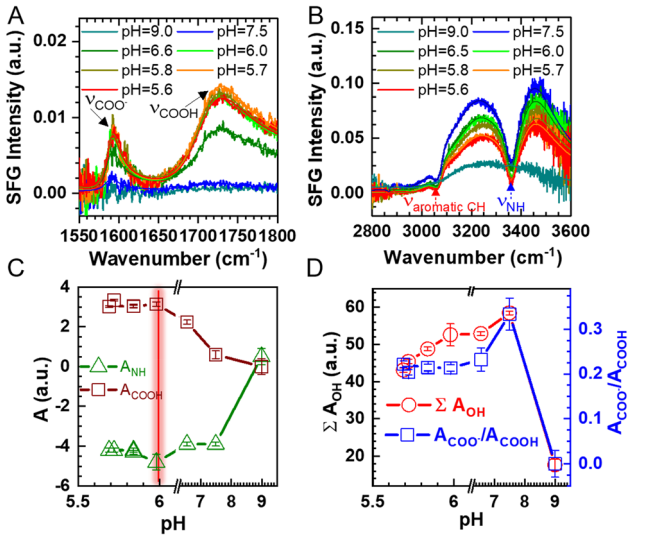

Fig. 4 Molecular structure and interaction for nucleation of diclofenac at the air–water interface. (A and B) SFG spectra in COO^-/COOH (A) and CH/OH (B) region for the diclofenac sodium at the air–water interface with varying pH, as derived from the titration curve. The spectra were recorded under SSP polarization (S-polarized SFG, S-polarized VIS, and P-polarized IR) combinations, and spectral fits (thinner lines) are superimposed. (C and D) Fitting analysis of the SFG spectra: (C) fitting amplitudes of the protonated ν_{COOH} band at ~1720 cm^{-1} in (A) (open wine square) and the NH band at ~3350 cm^{-1} in (B) (open green triangle), the red dashed line marks the saturation of amplitudes with pH < 6.0. (D) Sum of amplitudes for the hydrogen-bonded OH bands (open red circular), and the ratio of amplitudes for C=O bands in deprotonated ν_{COO^-} and protonated ν_{COOH} groups (open blue square). Error bars in (C) and (D) reflect the standard deviation of the fitting results.

We also recorded SFG spectra in CH/OH (2800–3600 cm^{-1}) frequency window, to probe the hydrophobic groups of diclofenac as well as interfacial water. Fig. 4(B) presents these spectra for the diclofenac sodium at the air–water interface with varying pH. Two vibrational bands from diclofenac molecules are clearly identified: namely, one at ~3060 cm^{-1} for the ν_2 mode of the phenyl ring,[32,35–37] and the other at ~3356 cm^{-1} for the N–H mode of the NH group. In addition to diclofenac bands, two broad OH bands dominate the spectra. These two OH bands, centered at ~3200 cm^{-1} and ~3450 cm^{-1}, can be assigned to the OH stretch from strongly and weakly hydrogen-bonded (H-bonded) water molecules, respectively.[38,39] Within the CH/OH spectra region, the aromatic CH and NH bands are often interfering, and thus overshadowed by broad OH bands. In accordance with previous literature,[40–42] the peak/dip feature of aromatic bands points to the positively and negatively charged surface, respectively. The aromatic bands in the spectra of Fig. 4(B) exhibit dips, indicating the presence of negatively charged diclofenac molecules at the water surface, which corresponds to the positive OH peaks. Accordingly, the apparent dephasing NH bands indicate their opposite, negative sign, with NH groups pointing, on average, toward the bulk. With decreasing pH to 7.5, the resonant diclofenac bands are clearly observable, and the intensity of OH bands increases significantly. The negatively charged diclofenac sodium molecules can polarize or align the OH dipoles of water in the diffuse layer, thereby giving rise to strong SFG signals.[43–48] For the charged interface, the OH SFG signal of water originates from both the interfacial layer ($\chi^{(2)}$-contribution) and the diffuse layer ($\chi^{(3)}$-contribution).[43–48] During titration, the ionic strength was kept constant. The 5 mM salt concentration corresponds to a Debye length of ~3 nm, implying a relatively large contribution from the diffuse layer.

The SFG spectra in Fig. 4(A and B) are further quantified by global fitting according to the equation below:

$$I_{SFG} \propto \left|\chi^{(2)}\right|^2 = \left|{\chi_{non_res}}^{(2)} + {\chi_{res}}^{(2)}\right|^2 = \left|A_{non_res} e^{i\Phi non_res} + \sum_{n=1}^{\infty} \frac{A_n}{\omega_{IR} - \omega_n + i\Gamma_n}\right|^2 \quad (1)$$

In eqn (1), the effective susceptibility $\chi^{(2)}$ consists of a non-resonance (${\chi_{non_res}}^{(2)}$) and a resonance (${\chi_{res}}^{(2)}$) term. A_{non_res} and ϕ_{non_res} are the amplitude and phase of the non-resonant signal, respectively. A_n is the amplitude of the resonant signal, ω_n the resonant frequency, ω_{IR} the infrared frequency and Γ_n the width of transition. Within the global fitting procedure, the resonant frequency (ω_n) and the width of vibrational transition (Γ_n) for each resonant band are all constrained to be the same for a series of spectra, obtaining different amplitudes (A_n) for a comparative study. Tables S2 and S3 present all fitting results. Fig. 4(C) presents the fitted amplitudes for the COOH and NH bands of diclofenac molecules. As explained above, the amplitudes of these bands have different signs, while showing similar trends with varying pH: the amplitudes increase with decreasing pH and saturate at pH = 5.6–6.0. Notably, according to previous studies,[49,50] the surface pK_a of organic acid at the air–

© 2025 The Author(s). Published by the Royal Society of Chemistry

Open Access Article. Published on 03 September 2025. Downloaded on 17/5/2026 9:18:33 AM. This article is licensed under a Creative Commons Attribution-NonCommercial 3.0 Unported Licence.

water interface can be well derived by evaluating the peak area of the protonated COOH and deprotonated COO^- bands. Unfortunately, the symmetric COO^- band is not observed in our spectra, similar to another recent study.[51] The antisymmetric COO^- band is rather weak, which does not allow rigorous determination of the surface pK_a of diclofenac. However, we observe a clear plateau for the amplitude of the protonated COOH band at pH = 5.6–6.0, which implies the surface pK_a is higher than this pH range – and apparently higher than the reported solution pK_a. In accordance with previous literature,[49–51] the surface pK_a is increased compared to the bulk. We assign this in part to the surface enrichment of protons,[52–56] this leads to an enhanced population of neutral diclofenac, which will promote nucleation. Fig. 4(D) presents the sum of the amplitudes (open red circles) for the two water OH bands, which reflects the degree of water alignment. The sum of amplitudes reaches a maximum at pH = 7.5, suggesting that the adsorption of charged diclofenac sodium molecules generates an electric field and aligns the water molecules at the interface. With decreasing pH further, the sum of amplitudes decreases, implying the decreasing alignment of water molecules, which is mainly caused by the reduced charge density due to the accumulation of neutral diclofenac molecules at the interface. The ratio of amplitudes for COO^- and COOH bands (open blue square) – reflecting charge density of diclofenac (*i.e.*, charged *vs.* neutral) – is also analyzed. The trend for the ratio of A_{COO^-}/A_{COOH} mimics that for the sum of OH amplitudes.

To complement our SFG study, we investigate the effect of air–water interfaces from MD simulations, we switched the previously discussed simulation cell from 3D to 2D periodic boundary conditions. The resulting slab model is illustrated in Fig. 5. Starting from the bulk solution of diclofenac PNCs, implementation of the air–water interface leads to rapid (ns-scale) alignment of the apolar diclofenac moieties at the boundaries to the vapor phase, and formation of a monolayer. After 100 ns relaxation, we furthermore observe distinct aggregation and de-solvation of diclofenac molecules, thus reflecting the onset of diclofenac nucleation out of the monolayer, moderating the air–water interface. Notably, the de-solvated, –COOH groups eventually form pair-wise hydrogen bonds between diclofenac molecules, resulting in dimers that are characteristic of the crystal structure of diclofenac.

The relaxed air–water interface was furthermore subjected to probing the deprotonation of diclofenac. For this, half of the interfacial diclofenac species were deprotonated whilst introducing the same number of sodium ions to the water phase for charge compensation (see SI and Fig. S8 for details). Upon further MD simulations, we observed the re-migration of deprotonated diclofenac into bulk water at the 10 ns scale – thus clearly demonstrating the disfavoring of deprotonation of diclofenac at the air–water interface.

The structure and rearrangement of diclofenac and water at the air–water interface are closely related to the promoted nucleation at this hydrophobic interface. To unravel the inherent driving force for the interfacial nucleation, we compare the nucleation in bulk solution and at the air–water interface. In bulk solution, we identify nanoscale PNCs, which, in accordance with nonclassical nucleation, have been detected in the nucleation of other organic APIs, such as ibuprofen.[26] Interestingly, these nanoscale PNCs of diclofenac are rather dynamic, as mediated by the interfacial interaction between PNCs and water.

Despite this stark contrast, our combined SFG and MD results reveal that protonated diclofenac molecules assemble into highly ordered motifs at the air–water interface, which, by enhancing hydrophobic contacts, lead to dimer structures

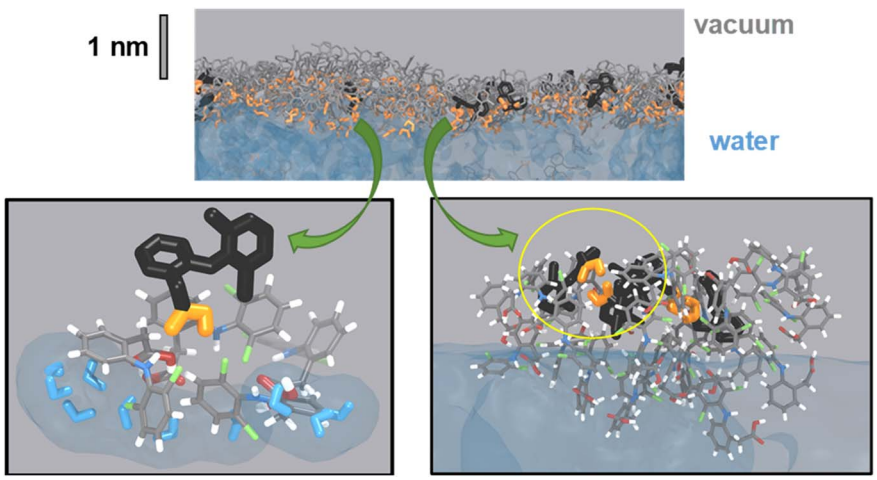

Fig. 5 Diclofenac assembly at the air–water interface. Implementation of a vacuum–water interface to the MD simulation model of bulk diclofenac PNC solution, followed by a 100 ns relaxation run at 300 K. The top panel shows an overview of the water–vacuum interface featured in the MD simulation, from which close-ups were depicted at the bottom. While a single solvent-separated diclofenac molecule is highlighted at the lower left, aggregation is shown at the lower right, respectively. Water is indicated in (transparent) blue, with explicit water molecules (blue sticks) only shown in the close-up at the lower left. In turn, diclofenac molecules in contact to water and separated from the solution are shown in gray and black, respectively, whilst explicit atom colors (H: white, C: gray, N: blue, O: red, Cl: green) is used in the close-ups. Note that nearby species of water-uncoordinated diclofenac readily form dimers by pair-wise hydrogen bonding of the –COOH groups (orange).

Open Access Article. Published on 03 September 2025. Downloaded on 17/5/2026 9:18:33 AM. This article is licensed under a Creative Commons Attribution-NonCommercial 3.0 Unported Licence.

characteristic of diclofenac crystals. In addition to increasing hydrophobic interactions, the adsorbed diclofenac dehydrates and reduces the number of coordinated water molecules, and, in parallel, decreases the charge density at the interface. Both these two scenarios result in decreased alignment of interfacial water, this seems to be in line with nonclassical nucleation: the additional entropy gained by water – from order to disorder – would also promote the interfacial nucleation process. Notably, our SFG data reveal a higher surface pK_a of diclofenac than that for bulk solution, and accordingly, the reduced ionic population of diclofenac, as consolidated by our MD data (Fig. S8), also contributes to the promoted nucleation at hydrophobic air–water interface.

3 Conclusions

We compared the nucleation of pharmaceutical diclofenac in bulk solution and at the air–water interface. In solution, the diclofenac molecules form dynamically ordered liquids like PNCs, which proceed in accordance with nonclassical PNCs pathways. Compared to bulk solution, the nucleation at interface occurs earlier during titration. The promoted nucleation at the interface is attributed to the highly ordered diclofenac–water motif. This enhances both hydrophobic contacts between diclofenac molecules, and supports the formation of hydrogen-bonded diclofenac pairs that fully separate from water and likely serve as crystal nuclei. In addition, reduced surface pK_a as compared to the bulk case leads to more protonated diclofenac at the interface, which further promotes nucleation. Our results provide molecular-level insights into the nucleation of API molecules, particularly highlighting the importance of hydrophobic interfaces during nucleation. Recognizing the molecular interactions at hydrophobic interfaces is crucial for controlling organic nucleation for various applications.

Author contributions

H. L., H. C. and M. B. conceived the research idea. H. L. conducted surface pressure, SFG, and analyzed the data, E. W. conducted cryo TEM experiment, M. M. and D. Z. performed MD simulations, D.-Z. Q. conducted BAM measurement. H. L., A. D., H. Z., H. C., and M. B. discussed and interpreted the results. H. L. wrote the manuscript with inputs from all co-authors.

Conflicts of interest

The authors declare no competing interests.

Data availability

The data that support the findings of this study are available from the corresponding authors upon reasonable request.

Supplementary information: Method description, analysis of surface pressure data, additional SFG spectra and analysis, description and additional analysis of MD simulations. See DOI: **https://doi.org/10.1039/d5sc03816b**.

Acknowledgements

We are grateful for the financial support from the MaxWater Initiative of the Max Planck Society. MM and DZ acknowledge funding by the DFG *via* grant ZA 420/15-1, and HL and HZ acknowledge the financial support from Zhejiang Province *via* the Top-Talent Program (Jiaxing University). The authors gratefully acknowledge the scientific support and HPC resources provided by the Erlangen National High Performance Computing Center (NHR@FAU) of the Friedrich-Alexander-Universität Erlangen-Nürnberg (FAU) under the NHR project b108dc. NHR funding is provided by federal and Bavarian state authorities. NHR@FAU hardware is partially funded by the German Research Foundation (DFG) – 440719683. Open Access funding provided by the Max Planck Society.

References

1 M. A. E. Yousef and V. R. Vangala, Pharmaceutical Cocrystals: Molecules, Crystals, Formulations, Medicines, *Cryst. Growth Des.*, 2019, **19**, 7420–7438.
2 I. J. Sugden, D. E. Braun, D. H. Bowskill, C. S. Adjiman and C. C. Pantelides, Efficient Screening of Coformers for Active Pharmaceutical Ingredient Cocrystallization, *Cryst. Growth Des.*, 2022, **22**, 4513–4527.
3 D. Erdemir, A. Y. Lee and A. S. Myerson, Nucleation of Crystals from Solution: Classical and Two-Step Models, *Acc. Chem. Res.*, 2019, **42**, 621–629.
4 J. Anwar and D. Zahn, Uncovering Molecular Processes in Crystal Nucleation and Growth by Using Molecular Simulation, *Angew. Chem., Int. Ed.*, 2011, **50**, 1996–2013.
5 D. Gebauer, J. D. Gale and H. Cölfen, Crystal Nucleation and Growth of Inorganic Ionic Materials from Aqueous Solution: Selected Recent Developments, and Implications, *Small*, 2022, **18**, 2107735.
6 D. Gebauer, P. Raiteri, J. D. Gale and H. Cölfen, On Classical and Nonclassical Views on Nucleation, *Am. J. Sci.*, 2018, **318**, 969–988.
7 D. Gebauer, M. Kellermeier, J. D. Gale, L. Bergstrom and H. Cölfen, Pre-Nucleation Clusters as Solute Precursors in Crystallization, *Chem. Soc. Rev.*, 2014, **43**, 2348–2371.
8 J. J. D. Yoreo, P. Gilbert, N. Sommerdijk, R. L. Penn, S. Whitelam, D. Joester, H. Zhang, J. D. Rimer, A. Navrotsky, J. F. Banfield, A. F. Wallace, F. M. Michel, F. C. Meldrum, H. Cölfen and P. M. Dove, Crystallization by Particle Attachment in Synthetic, Biogenic, and Geologic Environments, *Science*, 2015, **349**, aaa6760.
9 K. Henzler, E. O. Fetisov, M. Galib, M. D. Baer, B. A. Legg, C. Borca, J. M. Xto, S. Pin, J. L. Fulton, G. K. Schenter, N. Govind, J. I. Siepmann, C. J. Mundy, T. Huthwelker and J. J. D. Yoreo, Supersaturated Calcium Carbonate Solutions are Classical, *Sci. Adv.*, 2018, **4**, eaao6283.
10 C. H. Qian, G. Z. Zhu and L. S. Wang, Probing the Critical Dipole Moment to Support Excited Dipole-Bound States in Valence-Bound Anions, *J. Phys. Chem. Lett.*, 2019, **10**, 6472–6477.

© 2025 The Author(s). Published by the Royal Society of Chemistry

Open Access Article. Published on 03 September 2025. Downloaded on 17/5/2026 9:18:33 AM. This article is licensed under a Creative Commons Attribution-NonCommercial 3.0 Unported Licence.

11 P. J. M. Smeets, A. R. Finney, W. J. E. M. Habraken, F. Nudelman, H. Friedrich, J. Laven, J. J. D. Yoreo, P. M. Rodger and N. A. J. M. Sommerdijk, A Classical View on Nonclassical Nucleation, *Proc. Natl. Acad. Sci. U. S. A.*, 2017, **114**, E7882–E7890.
12 P. G. Vekilov, Two-Step Mechanism for the Nucleation of Crystals from Solution, *J. Cryst. Growth*, 2005, **275**, 65–76.
13 P. G. Vekilov, Nucleation, *Cryst. Growth Des.*, 2010, **10**, 5007–5019.
14 D. Gebauer, A. Völkel and H. Cölfen, Stable Prenucleation Calcium Carbonate Clusters, *Science*, 2008, **322**, 1819–1822.
15 E. R. Agudo, A. B. Cara, C. R. Agudo, A. I. Velasco, H. Cölfen and C. R. Navarro, A Nonclassical View on Calcium Oxalate Precipitation and the Role of Citrate, *Nat. Commun.*, 2017, **8**, 768.
16 J. Scheck, B. Wu, M. Drechsler, R. Rosenberg, A. E. S. V. Driessche, T. M. Stawski and D. Gebauer, The Molecular Mechanism of Iron(III) Oxide Nucleation, *J. Phys. Chem. Lett.*, 2016, **7**, 3123–3130.
17 M. J. Lukic, E. Wiedenbeck, H. Reiner and D. Gebauer, Chemical Trigger toward Phase Separation in the Aqueous Al(III) System Revealed, *Sci. Adv.*, 2020, **6**, eaba6878.
18 H. Hwang, Y. C. Cho, S. Lee, Y. Lee, S. Kim, Y. Kim, W. Jo, P. Duchstein, D. Zahn and G. W. Woo, Hydration Breaking and Chemical Ordering in a Levitated NaCl Solution Droplet beyond the Metastable Zone Width Limit: Evidence for the Early Stage of Two-Step Nucleation, *Chem. Sci.*, 2021, **12**, 179–187.
19 H. Lu, Y. C. Huang, J. Hunger, D. Gebauer, H. Cölfen and M. Bonn, Role of Water in $CaCO_3$ Biomineralization, *J. Am. Chem. Soc.*, 2021, **143**, 1758–1762.
20 P. Raiteri and J. D. Gale, Water Is the Key to Nonclassical Nucleation of Amorphous Calcium Carbonate, *J. Am. Chem. Soc.*, 2010, **132**, 17623–17634.
21 F. Sebastiani, S. L. P. Wolf, B. Born, T. Q. Luong, H. Cölfen, D. Gebauer and M. Havenith, Water Dynamics from THz Spectroscopy Reveal the Locus of a Liquid–Liquid Binodal Limit in Aqueous $CaCO_3$ Solutions, *Angew. Chem., Int. Ed.*, 2017, **56**, 490–495.
22 A. Soltani, D. Gebauer, L. Duschek, B. M. Fischer, H. Cölfen and M. Koch, Crystallization Caught in the Act with Terahertz Spectroscopy: Nonclassical Pathway for L-(+)-Tartaric Acid, *Chem. Eur J.*, 2017, **23**, 14128–14132.
23 A. F. Wallace, L. O. Hedges, A. F. Martinez, P. Raiteri, J. D. Gale, G. A. Waychunas, S. Whitelam, J. F. Banfield and J. J. D. Yoreo, Microscopic Evidence for Liquid-Liquid Separation in Supersaturated $CaCO_3$ Solutions, *Science*, 2013, **341**, 885–889.
24 H. Lu, M. Macht, R. Rosenberg, E. Wiedenbeck, M. Lukas, Q. Qi, D. Maltseva, D. Zahn, H. Cölfen and M. Bonn, Organic Nucleation: Water Rearrangement Reveals the Pathway of Ibuprofen, *Small*, 2024, **20**, 2307858.
25 D. Maltseva, S. Chatterjee, C. C. Yu, M. Brzezinski, Y. Nagata, G. Gonella, A. C. Murthy, J. C. Stachowiak, N. L. Fawzi, S. H. Parekh and M. Bonn, Fibril Formation and Ordering of Disordered FUS LC Driven by Hydrophobic Interactions, *Nat. Chem.*, 2023, **15**, 1146–1154.
26 C. Rafols, M. Roses and E. Bosch, A Comparison between Different Approaches to Estimate the Aqueous pK(a) Values of Several Non-Steroidal Anti-Inflammatory Drugs, *Anal. Chim. Acta*, 1997, **338**, 127–134.
27 J. Hadgraft, J. du Plessis and C. Goosen, The Selection of Non-Steroidal Anti-Inflammatory Agents for Dermal Delivery, *Int. J. Pharm.*, 2000, **207**, 31–37.
28 E. Wiedenbeck, M. Kovermann, D. Gebauer and H. Cölfen, Liquid Metastable Precursors of Ibuprofen as Aqueous Nucleation Intermediates, *Angew. Chem., Int. Ed.*, 2019, **58**, 19103–19109.
29 Y. Tsarfati, I. Biran, E. Wiedenbeck, L. Houben, H. Cölfen and B. Rybtchinski, Continuum Crystallization Model Derived from Pharmaceutical Crystallization Mechanisms, *ACS Cent. Sci.*, 2021, **7**, 900–908.
30 E. Wiedenbeck, Nucleation Precursors of Poorly Water-Soluble Pharmaceutical Compounds, PhD thesis, Konstanz University, 2019.
31 R. Demichelis, P. Raiteri, J. Gale, D. Quigley and D. Gebauer, Stable Pre-nucleation Mineral Clusters are Liquid-Like Ionic Polymers, *Nat. Commun.*, 2011, **2**, 590.
32 A. G. Lambert, P. B. Davies and D. J. Neivandt, Implementing the Theory of Sum Frequency Generation Vibrational Spectroscopy: A Tutorial Review, *Appl. Spectrosc. Rev.*, 2005, **40**, 103–145.
33 Y. R. Shen, *The Principles of Nonlinear Optics*, J. Wiley, 1984.
34 M. Bonn, Y. Nagata and E. H. G. Backus, Molecular Structure and Dynamics of Water at the Water-Air Interface Studied with Surface-Specific Vibrational Spectroscopy, *Angew. Chem., Int. Ed.*, 2015, **54**, 5560–5576.
35 N. Ji and Y. R. Shen, Sum Frequency Vibrational Spectroscopy of Leucine Molecules Adsorbed at Air-Water Interface, *J. Chem. Phys.*, 2004, **120**, 7107–7112.
36 T. Weidner, J. S. Apte, L. J. Gamble and D. G. Castner, Probing the Orientation and Conformation of Alpha-Helix and Beta-Strand Model Peptides on Self-Assembled Monolayers Using Sum Frequency Generation and NEXAFS Spectroscopy, *Langmuir*, 2010, **26**, 3433–3440.
37 T. Weidner, M. Dubey, N. F. Breen, J. Ash, J. E. Baio, C. Jaye, D. A. Fischer, G. P. Drobny and D. G. Castner, Direct Observation of Phenylalanine Orientations in Statherin Bound to Hydroxyapatite Surfaces, *J. Am. Chem. Soc.*, 2012, **134**, 8750–8753.
38 R. Pandey, K. Usui, R. A. Livingstone, S. A. Fischer, J. Pfaendtner, E. H. G. Backus, Y. Nagata, J. F. Nowoisky, L. Schmüser, S. Mauri, J. F. Scheel, D. A. Knopf, U. Pöschl, M. Bonn and T. Weidner, Ice-Nucleating Bacteria Control the Order and Dynamics of Interfacial Water, *Sci. Adv.*, 2016, **2**, e1501630.
39 Q. Du, E. Freysz and Y. R. Shen, Surface Vibrational Spectroscopic Studies of Hydrogen-Bonding and Hydrophobicity, *Science*, 1994, **264**, 826–828.
40 B. Braunschweig, F. Schulze-Zachau, E. Nagel, K. Engelhardt, S. Stoyanov, G. Gochev, K. Khristov, E. Mileva, D. Exerowa, R. Miller and W. Peukert, Specific effects of Ca(2+) ions and molecular structure of β-

Open Access Article. Published on 03 September 2025. Downloaded on 17/5/2026 9:18:33 AM. This article is licensed under a Creative Commons Attribution-NonCommercial 3.0 Unported Licence.

lactoglobulin interfacial layers that drive macroscopic foam stability, *Soft Matter*, 2016, **12**, 5995–6004.

41 K. Engelhardt, U. Weichsel, E. Kraft, D. Segets, W. Peukert and B. Braunschweig, Mixed Layers of β-Lactoglobulin and SDS at Air–Water Interfaces with Tunable Intermolecular Interactions, *J. Phys. Chem. B*, 2014, **118**, 4098–4105.

42 K. Meister, A. Paananen and H. J. Bakker, Identification of the Response of Protein N-H Vibrations in Vibrational Sum-Frequency Generation Spectroscopy of Aqueous Protein Films, *Phys. Chem. Chem. Phys.*, 2017, **19**, 10804–10807.

43 X. Zhao, S. Ong and K. B. Eisenthal, Polarization of Water Molecules at a Charged Interface. Second Harmonic Studies of Charged Monolayers at the Air/Water Interface, *Chem. Phys. Lett.*, 1993, **202**, 513–520.

44 S. Ong, X. Zhao and K. B. Eisenthal, Polarization of Water Molecules at a Charged Interface: Second Harmonic Studies of the Silica/Water Interface, *Chem. Phys. Lett.*, 1992, **191**, 327–335.

45 S. Pullanchery, T. L. Yang and P. S. Cremer, Introduction of Positive Charges into Zwitterionic Phospholipid Monolayers Disrupts Water Structure Whereas Negative Charges Enhances It, *J. Phys. Chem. B*, 2018, **122**, 12260–12270.

46 P. E. Ohno, H.-F. Wang and F. Geiger, Second-Order Spectral Lineshapes from Charged Interfaces, *Nat. Commun.*, 2017, **8**, 1032.

47 G. Gonella, C. Lutgebaucks, A. G. F. de Beer and S. Roke, Second Harmonic and Sum-Frequency Generation from Aqueous Interfaces Is Modulated by Interference, *J. Phys. Chem. C*, 2016, **120**, 9165–9173.

48 Y. C. Wen, S. Zha, X. Liu, S. Yang, P. Guo, G. Shi, H. Fang, Y. R. Shen and C. S. Tian, Unveiling Microscopic Structures of Charged Water Interfaces by Surface-Specific Vibrational Spectroscopy, *Phys. Rev. Lett.*, 2016, **116**, 016101.

49 B. A. Wellen, E. A. Lacha and H. C. Allen, Surface pKa of Octanoic, Nonanoic, and Decanoic Fatty Acids at the Air–Water Interface: Applications to Atmospheric Aerosol Chemistry, *Phys. Chem. Chem. Phys.*, 2017, **19**, 26551–26558.

50 S. Strazdaite, K. Meister and H. J. Bakker, Reduced Acid Dissociation of Amino-Acids at the Surface of Water, *J. Am. Chem. Soc.*, 2017, **139**, 3716–3720.

51 L. J. Musegades, O. P. Curtin and J. D. Cyran, Determining the Surface pKa of Perfluorooctanoic Acid, *J. Phys. Chem. C*, 2024, **128**, 1946–1951.

52 S. Das, S. Imoto, S. Sun, Y. Nagata, E. H. G. Backus and M. Bonn, Nature of Excess Hydrated Proton at the Water–Air Interface, *J. Am. Chem. Soc.*, 2020, **142**, 945–952.

53 S. Das, M. Bonn and E. H. G. Backus, The Surface Activity of the Hydrated Proton Is Substantially Higher than That of the Hydroxide Ion, *Angew. Chem., Int. Ed.*, 2019, **58**, 15636–15639.

54 V. Buch, A. Milet, R. Vacha, P. Jungwirth and J. P. Devlin, Water Surface is Acidic, *Proc. Natl. Acad. Sci. U. S. A.*, 2007, **104**, 7342–7347.

55 T. Ishiyama and A. Morita, Molecular Dynamics Analysis of Interfacial Structures and Sum Frequency Generation Spectra of Aqueous Hydrogen Halide Solutions, *J. Phys. Chem. A*, 2007, **111**, 9277–9285.

56 Y.-L. S. Tse, C. Chen, G. E. Lindberg, R. Kumar and G. Voth, Propensity of Hydrated Excess Protons and Hydroxide Anions for the Air–Water Interface, *J. Am. Chem. Soc.*, 2015, **137**, 12610–12616.

© 2025 The Author(s). Published by the Royal Society of Chemistry